Title
Ga[OSi(O t Bu) 3] 3 ·THF, a thermolytic molecular precursor for high surface area gallium-containing silica materials of controlled dispersion and stoichiometry

Journal
Dalton Transactions, 45(27)

ISSN
1477-9226

Authors
Dombrowski, James P
Johnson, Gregory R
Bell, Alexis T
et al.

Publication Date
2016-07-05

DOI
10.1039/c6dt01676f

Peer reviewed

Dalton Transactions

PAPER

View Article Online
View Journal | View Issue

Cite this: *Dalton Trans.*, 2016, **45**, 11025

$Ga[OSi(O^tBu)_3]_3$·THF, a thermolytic molecular precursor for high surface area gallium-containing silica materials of controlled dispersion and stoichiometry†

James P. Dombrowski,[a,c] Gregory R. Johnson,[b] Alexis T. Bell*[b,c] and T. Don Tilley*[a,c]

Received 29th April 2016,
Accepted 10th June 2016

DOI: 10.1039/c6dt01676f

www.rsc.org/dalton

The molecular precursor tris[(tri-*tert*-butoxy)siloxy]gallium, as the tetrahydrofuran adduct $Ga[OSi(O^tBu)_3]_3$·THF (**1**), was synthesized *via* the salt metathesis reaction of gallium trichloride with $NaOSi(O^tBu)_3$. This complex serves as a model for isolated gallium in a silica framework. Complex **1** decomposes thermally in hydrocarbon solvent, eliminating isobutylene, water, and *tert*-butanol to generate high surface area gallium-containing silica at low temperatures. When thermal decomposition was performed in the presence of P-123 Pluronic as a templating agent the generated material displayed uniform vermicular pores. Textural mesoporosity was evident in untemplated material. Co-thermolysis of **1** with $HOSi(O^tBu)_3$ in the presence of P-123 Pluronic led to materials with Ga : Si ratios ranging from 1 : 3 to 1 : 50, denoted **UCB1-GaSi$_3$**, **UCB1-GaSi$_{10}$**, **UCB1-GaSi$_{20}$** and **UCB1-GaSi$_{50}$**. After calcination at 500 °C these materials exhibited decreasing surface areas and broadening pore distributions with increasing silicon content, indicating a loss of template effects. The position and dispersion of the gallium in **UCB1-GaSi** materials was investigated using ^{71}Ga MAS-NMR, powder XRD, and STEM/EDS elemental mapping. The results indicate a high degree of gallium dispersion in all samples, with gallium oxide clusters or oligomers present at higher gallium content.

Introduction

Zeolitic and mesoporous gallium-containing materials have attracted interest as heterogeneous catalysts for a variety of industrially important transformations.[1] For example, zeolites containing gallium have been widely studied as catalysts for propane dehydrogenation to propene and propene aromatization, a reaction sequence commercialized as the Cyclar process.[1,2] It has been proposed that both framework gallium, *i.e.* gallium directly occupying a silicon position in the crystalline lattice, and extra-framework gallium play a role in this catalysis.[2] Mesoporous gallium-containing silicas have also been used as catalysts for several liquid phase reactions including epoxidation and Friedel–Crafts alkylation.[3–7] Interestingly, gallosilicates appear to exhibit catalytic properties that are different from those of comparable aluminosilicates, though the former are relatively less studied. For example, the Friedel–Crafts benzylation of benzene with benzyl chloride occurs readily over gallium-incorporated mesoporous silicas, while the aluminum analog is significantly less active.[7,8] The reverse is found when benzyl alcohol is used as the alkylating reagent.[7] These differences suggest that additional study of gallium-containing silicas may yield important new discoveries in catalysis.

A better understanding of the chemical properties associated with gallium centers should result from studies of gallium siloxide molecular models, or molecular chemistry designed to provide well-defined, single-site gallium materials. However, few molecular gallium siloxides are known, and none have been used to generate gallium-containing silica materials.[9,10] This laboratory has employed a synthetic strategy, termed the thermolytic molecular precursor (TMP) method, to utilize appropriately designed molecular complexes that serve as spectroscopic and structural models for an active site, and as precursors to materials that possess such active

[a]*Department of Chemistry, University of California, Berkeley, Berkeley, California 94720-1460, USA. E-mail: tdtilley@berkeley.edu*
[b]*Department of Chemical and Biomolecular Engineering, University of California, Berkeley, Berkeley, California 94720-1460, USA*
[c]*Chemical Sciences Division, Lawrence Berkeley Laboratory, 1 Cyclotron Road, Berkeley, California 94720, USA*

†Electronic supplementary information (ESI) available: NMR spectra of molecular precursors, vibrational spectroscopy of precursors, powder XRD patterns of all materials, HAADF-STEM images of all materials, crystallographic data, TG/DTA data of precursor mixtures. CCDC 1477192. For ESI and crystallographic data in CIF or other electronic format see DOI: 10.1039/c6dt01676f

sites. This approach starts with an oxygen-rich molecular precursor containing the active core of interest, using ligands that model the oxide support. For example, a M–O–SiO_3 moiety is modeled by a M–O–Si(O^tBu)$_3$ linkage. Such tri(*tert*-butoxy) siloxy complexes have been found to readily provide access to materials containing M[–O–SiO_3]$_n$ sites, *via* thermal elimination of isobutene and water.[11] These precursors have been used to generate bulk materials with high dispersion of the metal sites, or in surface modification reactions that introduce such sites onto an oxide support.[12]

This report describes a new molecular precursor, a tetrahydrofuran adduct of tris[(tri-*tert*-butoxy)siloxy]gallium, Ga[OSi(O^tBu)$_3$]$_3$·THF (**1**), as a thermolytic precursor to gallium-containing silica materials. Compound **1** represents the first precursor to gallium-silica materials containing solely Ga–O–SiO_3 covalent linkages and serves as a good spectroscopic model for gallium isolated on silica. As detailed below, complex **1** is also an effective, low-temperature precursor to gallium-silica materials with variable Ga : Si ratios of 1 : 3 to 1 : 50. This TMP method is suitable for use with a templating agent, P-123 Pluronic, which allows some control over the material's surface area and morphology.

Experimental

General

All synthetic manipulations were performed under a nitrogen atmosphere using Schlenk techniques or in a glovebox, unless otherwise noted. Tetrahydrofuran (unstabilized, Macron), pentane (Fisher Chemical HPLC grade) and toluene (Fisher Chemical HPLC Grade) were dried using a JC Meyer Solvent Column system and used without further treatment. Benzene-d_6 and toluene-d_8 were used for all NMR experiments and were deoxygenated with three freeze–pump–thaw cycles and dried for a minimum of 24 h over 3 Å molecular sieves before use. Calcinations were performed in a Lindberg 1200 °C three-zone tube furnace with a flow rate of 100 cm^3 min^{-1} using oxygen (99.96%). Gallium trichloride (99.999%, Strem Chemical) was stored in a glovebox and used without further purification. HOSi(O^tBu)$_3$, NaOSi(O^tBu)$_3$ and SBA-15 were synthesized by literature methods.[12–14]

Characterization

^{1}H and ^{13}C NMR spectra were collected on a Bruker AVB-400 NMR spectrometer at 400 MHz referenced internally to tetramethylsilane. All 2D-NMR spectra were collected on a Bruker AV-500 NMR spectrometer at 500 MHz. ^{29}Si NMR spectra were collected on a Bruker AV-600 NMR spectrometer at 600 MHz. IR spectra were collected on a Thermo Nicolet 6700 FTIR spectrometer using NaCl as a background and a pentane film of **1** between NaCl plates as the sample. Raman spectra were collected on a Horiba Yvon Jobin labRAM HR confocal Raman spectrometer with a wavelength of 633 nm. Thermogravimetric analyses were performed on a Seiko Instruments Inc. EXSTAR 6000 series TG/DTA 6300 under a gas flow of 100 cm^3 min^{-1} and a ramp rate of 10 °C min^{-1}. Powder X-ray diffraction data was collected at the University of California-Berkeley, CHEXRAY instrumentation facility using a D8 Discover GADDS Powder XRD instrument with a fine-focus sealed source (Cu-Kα radiation). Ammonia-TPD measurements were performed at the Center for the Development of Precision Chemical Materials housed at Chonnam National University.

Single-crystal X-ray crystallography

Single-crystal X-ray studies were performed at the University of California-Berkeley CHEXRAY instrumentation facility using an Apex II Quazar instrument with a microfocus sealed source (Incoatec IμS; Mo-Kα radiation, λ = 0.71073 Å). Measurements were taken on a Bruker APEX II CCD area detector and the data collection was computed and integrated using the Bruker APEX2 software package. Bruker SAINT was used for cell refinement and data reduction. The structure was solved using SHELXS-97 (Sheldrick 2008) and was refined using SHELXL-2013 (Sheldrick 2013). A 0.06 mm × 0.08 mm × 0.14 mm colorless plate-like crystal was used for the X-ray analyses in a frozen glass of paratone N hydrocarbon oil at 100(2) K under a flow of nitrogen.

HAADF-STEM and STEM/EDS elemental mapping

Imaging by high-angle annular dark-field scanning transmission electron microscopy (HAADF-STEM) and scanning transmission electron microscopy energy dispersive spectroscopy (STEM-EDS) was performed at the Molecular Foundry at the Lawrence Berkeley National Laboratory using an FEI Titan electron microscope. Samples were prepared for imaging by drop-casting 5 μL of an ethanol suspension of the sample particles onto a lacey carbon Cu TEM grid. The grids were then dried in a vacuum oven at 383 K for 1 h to evaporate the solvent. All imaging was performed using a 200 kV accelerating voltage. Elemental mapping by STEM-EDS was conducted using a Bruker silicon drift detector that collected fluorescent X-rays from 0 to 20 keV with a 140 eV energy resolution and 10 eV per channel dispersion. Processing and quantification of the elemental maps was done using the Bruker Esprit software program.

^{71}Ga MAS-NMR spectroscopy

Solid state ^{71}Ga MAS-NMR spectroscopy was performed at the NMR Facility at the University of California, Davis. The samples were run on a Bruker AVANCE 500 wide-bore NMR spectrometer equipped with a 11.74 T magnet. After hydration in a saturated water atmosphere for a minimum of 48 h, samples were packed into a 2.5 mm rotor for analysis. A 2.5 mm probe was used. A single pulse of 0.31 μs pulse length (corresponding to 45° tip-angle) and a relaxation delay of 0.1 s were used for data acquisition. Chemical shifts were externally referenced to a gallium trichloride solution. All samples were run at 34 kHz. **UCB1-GaSi$_3$** was run with a dwell time of 1 μs and 441 490 scans, **UCB1-GaSi$_{10}$** was run with a dwell time of 1 μs and 565 621 scans, **UCB1-GaSi$_{50}$** was run with a dwell time of 5 μs and 498 390 scans.

In situ FTIR spectroscopy with pyridine

In situ pyridine adsorption followed by FTIR spectroscopy was performed using a Nicolet 6700 FTIR spectrometer equipped with a Praying Mantis DRIFTS cell attachment (Harrick). Samples were diluted with potassium bromide and loaded into the DRIFTS cup of the High Temperature Reaction Chamber. Samples were pretreated at 120 °C for a minimum of 150 minutes under He flow (20 mL min^{-1}) before 2 μL of pyridine was vaporized into the He carrier gas and passed through the sample. Spectra were recorded post-injection until no changes between sequential spectra were observed. The areas of absorbance bands corresponding to Brønsted acid sites (~1545) and Lewis acid sites (~1455) were determined from the subtraction result of spectra taken after helium treatment at 120 °C and after pyridine adsorption signals had stabilized.[15] The Brønsted/Lewis acid site ratios were calculated using the peak areas and their respective molar extinction coefficients.[16]

Synthesis of $Ga[OSi(O^tBu)_3]_3$·THF (1)

A 30 mL THF solution of $Na[OSi(O^tBu)_3]_3$ (2.156 g, 7.53 mmol) was added dropwise over ten minutes to a 100 mL glass round-bottom Schlenk flask containing a stirred solution of $GaCl_3$ (0.465 g, 2.64 mmol) in 10 mL of THF. During addition, an opaque white suspension formed. After 90 minutes the solution was evaporated to dryness *in vacuo* leaving a white to pale-yellow solid. Extraction with pentane and filtration followed by evaporation to dryness *in vacuo* yielded a white solid (74% yield, 1.72 g, 1.85 mmol). Recrystallization from THF at −30 °C gave colorless crystals suitable for X-ray crystallography. Anal. Calcd for $C_{40}H_{89}GaO_{13}Si_3$: C, 51.54; H, 9.62. Found: C, 51.42; H, 9.72. IR (pentane film between NaCl plates, KBr beamsplitter, 500–3500 cm^{-1}): 2972 s, 2929 wsh, 2872 wsh, 1460 w, 1387 w, 1363 m, 1238 msh, 1217 w, 1196 s, 1103 wsh, 1051 vs, 1026 ssh, 912 wbr, 864 wbr, 829 m, 804 vw, 702 m, 665 w, 515 w. Raman (633 nm laser, 100–2000 cm^{-1}): 1448 s, 1239 m, 1191 wsh, 1030 wbr, 907 msh, 824 wsh, 800 ssh, 650 m, 535 w, ^1H NMR (benzene-d_6, 400 MHz, 20 °C): δ 1.51 (s, 81H, O^tBu, 4H, *THF overlapping*), δ 4.42 (bs, 4H, *THF*). $^{13}C\{^1H\}$ NMR (benzene-d_6, 400 MHz, 20 °C): δ 72.20 (*THF*), δ 32.41 (SiO^tBu), δ 25.34 (*THF*). ^{29}Si NMR (benzene-d_6, 600 MHz, 20 °C): δ −94.75.

Synthesis of UCB1-$GaSi_3$ material

In a typical preparation, in a drybox 0.600 g of **1** was dissolved in a solution of 0.200 g of P-123 Pluronic in 6 mL of dry toluene. This solution was then transferred to a 10 mL glass ampule interfaced to a glass tube with a 14/20 ground-glass joint and a Teflon stopper through a Cajon adapter. The apparatus was sealed under nitrogen, removed from the glovebox, and transferred to a Schlenk line. Three freeze–pump–thaw cycles were performed before the ampule was flame-sealed under vacuum while still frozen to prevent over-pressurization during thermolysis. After warming to room temperature, the sealed ampule was placed in a 135 °C oil bath for 24 h to produce a solid pale-yellow gel. After cooling to room temperature the ampule was ruptured and the contents were emptied onto an evaporation dish to air dry. After three days the remaining solids were calcined at 500 °C under O_2 for 3 h. The solids were collected, ground with a mortar and pestle to form a powder, and dehydrated at 120 °C under dynamic vacuum for 12 h before being stored in a glovebox. Anal. Calcd for Ga_2O_3·$3SiO_2$: Ga, 25.45; Si, 30.75. Found: Ga, 22.2; Si, 28.2, C, 1.53; H, 0.85 (corresponds to a Ga : Si ratio of 1 : 3.16).

Synthesis of UCB1-GaSi materials with lower gallium content

A mixture of **1** and tris(*tert*-butoxy)silanol (0.600 g),) with the ratios adjusted to afford the desired stoichiometry, was dissolved in a solution of 0.200 *g* of P-123 Pluronic in 6 mL of dry toluene. This solution was then transferred to a 10 mL glass ampule interfaced to a glass tube with a 14/20 ground glass joint and a Teflon stopper through a Cajon adapter. The apparatus was removed from the glovebox, sealed under nitrogen, and transferred to a Schlenk line. Three freeze–pump–thaw cycles were performed before the ampule was flame-sealed under vacuum while still frozen to prevent over-pressurization during precursor thermolysis. After warming to room temperature the sealed ampule was placed in an oil bath at 135 °C for 24 h, which resulted in the formation of a pale yellow gel. After cooling to room temperature the ampule was ruptured and the contents were emptied onto an evaporation dish to air dry. After three days the remaining solids were calcined at 500 °C under O_2 for 3 h. The solids were collected, ground by mortar and pestle to a powder, and dehydrated at 120 °C under dynamic vacuum for 12 h before being stored in a glovebox.

Anal. Calcd for Ga_2O_3·$20SiO_2$: Ga, 10.04; Si, 40.44. Found: Ga, 8.18; Si, 32.5, C, 0.61; H, <0.2 (corresponds to a Ga : Si ratio of 1 : 9.54).

Anal. Calcd for Ga_2O_3·$40SiO_2$: Ga, 5.38; Si, 43.36. Found: Ga, 4.81; Si, 38.7, C, 0.42; H, <0.2 (corresponds to a Ga : Si ratio of 1 : 20.0).

Anal. Calcd for Ga_2O_3·$100SiO_2$: Ga, 2.25; Si, 45.33. Found: Ga, 1.95; Si, 38.8, C, 0.16; H, <0.2 (corresponds to a Ga : Si ratio of 1 : 49.4).

Synthesis of untemplated Ga_2O_3·$3SiO_2$ material

In a typical preparation, 0.600 g of **1** was dissolved in 6 mL of dry toluene. This solution was then transferred to a 10 mL glass ampule interfaced to a glass tube with a 14/20 ground glass joint and a Teflon stopper through a Cajon adapter. The apparatus was removed from the glovebox, sealed under nitrogen, and transferred to a Schlenk line. Three freeze–pump–thaw cycles were performed before the ampule was flame-sealed under vacuum while still frozen to prevent over-pressurization during precursor thermolysis After warming to room temperature, the sealed ampule was placed in an oil bath pre-heated to 135 °C for 24 h. During this time, depending on the sample, a clear, pale yellow gel formed. After cooling to room temperature the ampule was ruptured and the contents were emptied onto an evaporation dish to air dry. After three days the remaining solids were calcined at 500 °C under O_2 for 3 h. The solids were then collected, ground with a mortar and

pestle to a powder, and dehydrated at 120 °C under dynamic vacuum for 12 h before being stored in a glovebox.

Results & discussion

Synthesis of 1

The complex $Ga[OSi(O^tBu)_3]_3$·THF (**1**) was synthesized by addition of 2.9 equivalents of sodium tris(*tert*-butoxy)silanolate to gallium trichloride in THF. Following evaporation and extraction with pentane, the product was recrystallized from THF as analytically pure colorless crystals in 74% yield (Scheme 1).

Single-crystal X-ray crystallographic characterization of 1

Single, plate-like crystals of **1** were obtained by recrystallization from a concentrated THF solution at −30 °C. X-ray crystallographic analysis confirmed the complex to be the monomeric THF adduct. Unfortunately, the structure exhibited total molecular disorder, which prevents determination of precise bond-lengths and angles; however, it is clear the gallium and silicon atoms adopt approximately tetrahedral coordination and a THF molecule is bound to the gallium center (Fig. 1).

Stability and relevance of 1 as a thermolytic molecular precursor

The molecular precursor **1** fills a vacancy in the series of group 13 tris(tri-*tert*-butoxy)siloxide complexes in that similar derivatives have previously been reported for boron, aluminum and indium.[9,17,18] Complexes of each type have been successfully investigated as thermolytic precursors to group 13 element-containing silica materials. Of the few reports regarding gallium siloxide complexes, only one has described their use as thermolytic precursors. Driess *et al.* reported the syntheses of $[Me_2Ga(OSiEt_3)]_2$ and $[Me_2Ga(OSi(O^tBu)_3)]_2$; however, thermolysis of these compounds gave gallium oxide rather than gallium-containing silica.[9] Therefore, development of a well-defined precursor for the thermolytic formation of gallium-containing silicas has remained an unrealized goal.

The molecular precursor **1** is air-sensitive and thermally unstable at room temperature. Treatment of **1** with one equivalent of water led to partial hydrolysis of the gallium–oxygen bonds. A ^{1}H NMR spectrum recorded 15 minutes after addition of one equivalent of water to a solution of **1** in benzene-d_6 shows resonances diagnostic of tris(*tert*-butoxy)-silanol and THF. An insoluble material, presumably hydrated gallium oxide, was observed in the NMR tube. Monitoring a benzene-d_6 solution of complex **1** by ^{1}H NMR spectroscopy revealed that the complex began to thermally decompose within six hours at 20 °C, with generation of a trace amount of isobutene. Note that the aluminum analog of **1** also decomposes at 20 °C with elimination of isobutene.[18] Over 21 h at 20 °C, decomposition of **1** in benzene-d_6 occurred with the formation of free tris(*tert*-butoxy)silanol and isobutene (3.9% and 7.4% of available *tert*-butoxy groups, respectively) and concurrent deposition of a gel. In the solid state, **1** begins to decompose within six hours at 20 °C, indicated by the formation of hydrocarbon-insoluble material.

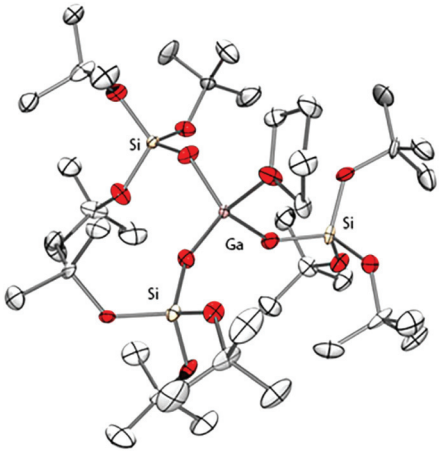

Fig. 1 Thermal ellipsoid plot of **1** at the 40% probability level. The hydrogen atoms are omitted for clarity.

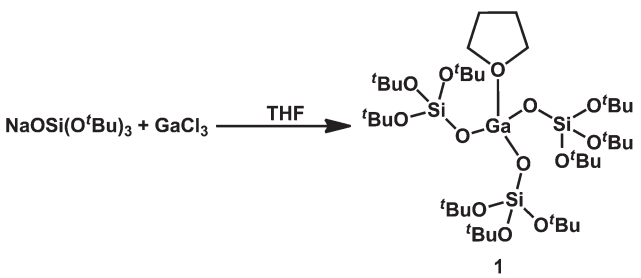

Scheme 1 Synthesis of $Ga[OSi(O^tBu)_3]_3$·THF (**1**).

Thermogravimetric (TG/DTA) and NMR spectroscopic analyses of 1

The thermal instability observed at 20 °C suggested that **1** may be a thermolytic molecular precursor (TMP) to gallium-silica materials. Thermogravimetric analysis of **1** under O_2 or N_2 indicated rapid mass loss associated with thermal decomposition of the precursor around 110 °C (Fig. 2). Isobutylene formation is expected during this event based on ^{1}H NMR experiments discussed above as well as previous studies, which established the mechanism for thermolytic decomposition of similar group 13 precursors.[19] The tailing mass losses from ~170–1000 °C can be attributed to a loss of water generated during silanol condensation. The lack of any additional major mass-loss events before 1000 °C indicated that coordinated THF must have evaporated during the elimination of *tert*-butoxy groups from **1**. Indeed, the total mass loss (76.8%) is close to the expected value for loss of 9 equivalents of isobutylene, 4.5 equivalents of water and coordinated THF (required losses for the complex to form Ga_2O_3·$6SiO_2$: 70.6%).

Additional insight into the thermal decomposition was gained through NMR spectroscopic observation of soluble decomposition products. The gallium precursor **1** in toluene-

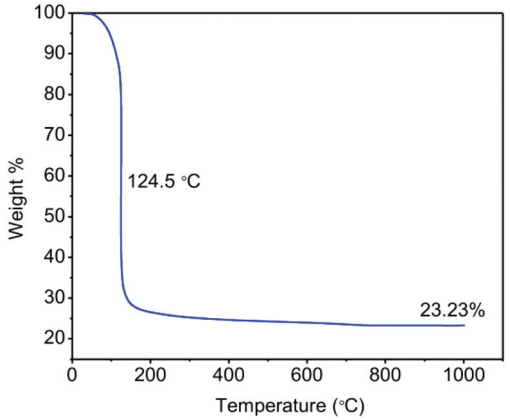

Fig. 2 TGA mass-loss curve for **1** under nitrogen.

d_8 was heated to 135 °C for 24 h, resulting in the total disappearance of signals associated with **1** (by ^{1}H NMR spectroscopy) along with a complicated mixture of organic products, potentially due to additional reactivity between the gallium centers and isobutene or *tert*-butanol. In addition, a gallium-silica gel formed in the NMR tube. The elimination products generated over the first 30 minutes of thermolysis were collected by vacuum transfer from a sample of **1** that was heated (135 °C) under vacuum. The volatile products were deposited onto frozen benzene-d_6 at −196 °C containing ferrocene as an internal standard. By ^{1}H NMR spectroscopy, isobutene, *tert*-butanol, THF, and water were the major volatile products accounting for 38% of the *tert*-butoxy groups and 54% of the THF present in the sample. These observations are consistent with previous studies on related TMP complexes containing tri-(*tert*-butoxy)siloxide groups.[11,17,18]

In contrast to the clean thermolysis observed for **1**, the gallium siloxides $[Me_2Ga(OSiEt_3)]_2$ and $[Me_2Ga(OSi(O^tBu)_3)]_2$ investigated by Driess and coworkers exhibit complex multistep thermal degradations at high temperatures, which result in gallium oxide formation.[9] Comparing the reactivity of **1** to $[Me_2Ga(OSiEt_3)]_2$ and $[Me_2Ga(OSi(O^tBu)_3)]_2$ suggests that the methyl groups on gallium may interfere with the mechanism for formation of gallium-silica materials.

Synthesis of gallium-containing silica materials

Initial investigations into the synthesis of gallium-containing silica materials using **1** as a thermolytic molecular precursor were performed by heating **1** in either a solution of toluene or toluene/P-123 Pluronic at 135 °C. To remove the P-123 Pluronic and drive off residual solvent after thermolysis, the resulting gels were air-dried for three days to form white or pale yellow monoliths that were then calcined at 500 °C in O_2 for three hours. The white calcined samples were then ground to a powder by mortar and pestle. This synthetic protocol involving P-123 Pluronic as template has previously been reported by this laboratory to generate materials with uniform pore distributions and narrow pore diameters.[20]

Dinitrogen-physisorption measurements were performed on calcined samples of P-123-templated and untemplated materials generated from solution thermolyses of **1** (**UCB1-GaSi$_3$** and **Ga$_2$O$_3$·6SiO$_2$**, respectively). These measurements indicated the presence of template effects for **UCB1-GaSi$_3$**, as previously observed for several other UCB1 materials.[20] High surface areas were observed for both samples (636 $m^2\ g^{-1}$ and 507 $m^2\ g^{-1}$ for **UCB1-GaSi$_3$** and **Ga$_2$O$_3$·6SiO$_2$** respectively), with **UCB1-GaSi$_3$** having a much smaller average pore radius and a narrower pore distribution. In addition, the dinitrogen-physisorption measurement for un-templated **Ga$_2$O$_3$·6SiO$_2$** exhibited a shift in the hysteresis loop to significantly higher relative pressures, indicative of textural mesoporosity rather than the vermicular pores reported for **UCB1** materials (Fig. 3).[21]

Powder X-ray diffraction (pXRD) experiments were performed to look for evidence of crystalline oxide domains in **UCB1-GaSi$_3$** and **Ga$_2$O$_3$·6SiO$_2$**. The results indicate that materials formed by direct thermolysis of **1** exhibit broad, shoulder peaks at 2θ = ~35° and ~65° (see ESI, S5†). These features are largely unchanged between the templated and untemplated materials and lie in the general region for α-, γ-, δ-, ε- and β-Ga_2O_3; however, the broadness of the peaks prevents definitive assignments.[22] These peaks were observed in pXRD spectra of **UCB1-GaSi$_3$** samples calcined at temperatures as low as 200 °C, which is above the expected decomposition temperature of P-123, but were not observed in the uncalcined samples (see ESI, S7†).[23] Calcination of **UCB1-GaSi$_3$** at higher temperatures (800 °C) resulted in growth of peaks associated with γ-Ga_2O_3. It is not clear whether the higher temperature treatment leads to formation of larger particles of the same oxide phase observed at 500 °C or new, different phases.[22,24]

The observation that direct thermolysis of **1** leads to formation of gallium-silica materials with small gallium oxide domains was not unexpected given the relatively high Ga : Si molar ratio dictated by the precursor. Thus to promote isolated gallium sites it was of interest to examine **UCB1-GaSi** materials

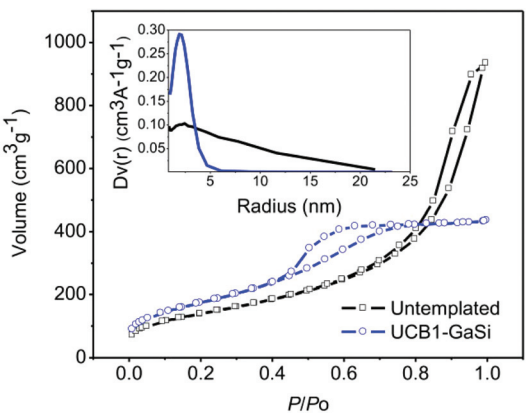

Fig. 3 Nitrogen adsorption–desorption isotherms and pore size distributions (as change in pore volume with respect to pore radius, inset, BJH desorption method) after calcination at 500 °C in O_2 for untemplated gallium-silica (**Ga$_2$O$_3$·6SiO$_2$**) and P-123-templated gallium-silica (**UCB1-GaSi$_3$**).

having higher contents of silicon, and in this regard it seemed possible to tune the gallium content by inclusion of a purely siliceous precursor during thermolysis.

Tris(*tert*-butoxy)silanol was selected as a siliceous diluent since it contains only *tert*-butoxy and hydroxyl substituents on silicon that are readily lost in the thermolysis/condensation process. Previous investigations into the co-thermolysis of tris(*tert*-butoxy)silanol with a tantalum(v) precursor, $Ta(O^iPr)_2[OSi(O^tBu)_3]_3$, found that over a narrow range of Ta : Si ratios complete incorporation of the precursors into the materials occurs.[25] However, incomplete thermolysis of added tris(*tert*-butoxy)silanol was observed if the Ta : Si ratio of the combined precursors decreased below 1 : 9.[25] This co-thermolysis approach was applied to generate materials with tunable Ga/Si ratios in the presence of the P-123 Pluronic template with the goal of controlling the coordinate environment of the gallium centers.

The co-thermolysis of **1** with tris(*tert*-butoxy)silanol occurred in toluene in the presence of P-123 Pluronic by a method analogous to that used for the synthesis of **UCB1-GaSi$_3$**. The as-synthesized gels, once air-dried, were calcined at 500 °C in O_2 to give materials with Ga : Si ratios of 1 : 10, 1 : 20, and 1 : 50, denoted **UCB1-GaSi$_{10}$**, **UCB1-GaSi$_{20}$**, and **UCB1-GaSi$_{50}$**, respectively. Elemental analysis of the gallium to silicon ratios confirmed that the intended stoichiometries were achieved (Table 1). The accuracy with which gallium contents may be targeted by this method is noteworthy, since hydrothermal syntheses of gallium-containing silica by direct addition of a gallium precursor to a silica sol–gel often display lower than anticipated loadings in the final material.[26–29] The thermolytic method employed here, therefore, provides valuable access to gallium-containing silica over a broad range of precise loadings.

As a reminder, tris(*tert*-butoxy)silanol boils above 205 °C, therefore the observation of expected Ga : Si ratios following calcination is significant.[30] This result provides evidence of total precursor decomposition and incorporation into the gel during the co-thermolysis; any remaining free silanol would be expected to boil out during calcination which would result in higher Ga : Si ratios than targeted.

NMR investigations were performed to monitor the thermolysis of both tris(*tert*-butoxy)silanol and **1** in solution for completion. Thermolysis in toluene-d_8 under gelation conditions (135 °C for 24 h) produced isobutene and small amounts of *tert*-butanol as the major soluble products even at the lowest loading of gallium, indicating complete consumption of the precursors (see ESI, S8†).

The wide range of metal loadings achievable using **1** as the metal-containing precursor stands in contrast to the previous work on tantala-silica materials described above. Addition of catalytic amounts of aluminum trichloride to TMP thermolysis reactions is known to induce thermolysis and decrease gelation times, and it appears that the gallium Lewis-acid centers present in **1** also exhibit an ability to catalyze the thermal decomposition even at low loadings.[19,20,31]

Powder X-ray diffraction (pXRD) studies of the newly synthesized **UCB1-GaSi** materials with lower Ga : Si ratios (denoted **UCB1-GaSi$_{10}$**, **UCB1-GaSi$_{20}$**, and **UCB1-GaSi$_{50}$**) revealed that the shoulder peaks observed in **UCB1-GaSi$_3$** were absent. This indicates that the dilution was successful in modulating the formation of gallium oxide domains (see ESI, S6†).

To investigate the dilution method using tris(*tert*-butoxy)silanol as a means for suppressing the formation of gallium oxide, ^{71}Ga MAS-NMR spectroscopy was performed on calcined **UCB1-GaSi$_3$**, **UCB1-GaSi$_{10}$**, and **UCB1-GaSi$_{50}$**. The presence of only tetrahedral gallium signals in lower gallium-loading materials supports the elimination of large gallium oxide crystallites in favor of tetrahedrally-coordinated gallium atoms embedded in silica (Fig. 4). However, note that previous reports suggest that not all gallium is necessarily observable by NMR, especially if the gallium environments possess low symmetry or high disorder.[26] Hydration of gallium silicates has been reported to assist in relaxing signals and sharpening peaks; therefore, these samples were stored under a saturated water atmosphere for a minimum of 48 h prior to analysis.[26]

Table 1 Elemental analyses and physisorption parameters for synthesized materials

Material	Ga : Si[a]	SA (m^2 g^{-1})	Ave. pore radius (nm)	Pore vol. (cm^3 g^{-1})
UCB1-GaSi$_3$	1 : 3(3.16)	636	2.0	0.65
UCB1-GaSi$_{10}$	1 : 10(9.54)	497	3.9	0.99
UCB1-GaSi$_{20}$	1 : 20(20.0)	379	7.2	1.25
UCB1-GaSi$_{50}$	1 : 50(49.4)	293	13.7	1.57
Untemplated	1 : 3	507	5.3	1.44

[a] Values in parentheses indicate measured ratios.

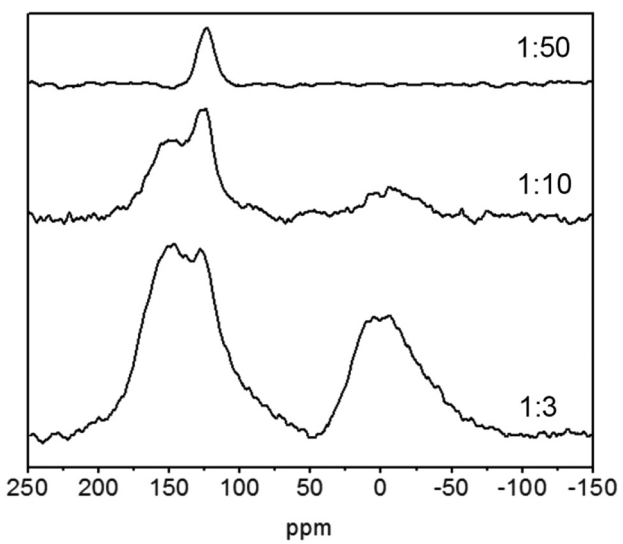

Fig. 4 ^{71}Ga-MASNMR spectra of **UCB1-GaSi$_3$** (1 : 3), **UCB1-GaSi$_{10}$** (1 : 10) and **UCB1-GaSi$_{50}$** (1 : 50) after calcination at 500 °C in O_2. Signals for tetrahedral coordination (~150 ppm and ~123 ppm) and octahedral coordination (~0 ppm) are apparent.

The results indicate the presence of two major peaks for tetrahedral gallium with maxima at ~123 and ~150 ppm along with a peak for octahedral gallium at ~0 ppm in the **UCB1-GaSi$_3$** and **UCB1-GaSi$_{10}$** samples. For **UCB1-GaSi$_{50}$** only the peak at ~123 ppm is present in the ^{71}Ga MAS-NMR spectrum.

The broad signals present at ~150 and ~0 ppm in gallium-rich **UCB1-GaSi** samples are similar to literature reports of ^{71}Ga NMR shifts for γ-Ga_2O_3, and are tentatively assigned to this oxide phase.[32] They are inconsistent with gallium oxyhydroxide structures which would be expected to exhibit only signals attributed to octahedral Ga and have signals upfield from those reported for β-Ga_2O_3.[33] The sharp signal at ~123 ppm was present in all three samples and was the only observable signal in **UCB1-GaSi$_{50}$**. This peak is tentatively assigned to an isolated gallium species; however, earlier reports of "single-site" gallium on MCM-41 or SBA-15 describe a different tetrahedral signal located at ~150 ppm.[26,28] This indicates that the **UCB1-GaSi** materials may possess a different type of isolated species.

Elemental mapping STEM/EDS spectroscopy was performed on **UCB1-GaSi$_3$** and **UCB1-GaSi$_{10}$** samples. No visible signs of the phase segregation of gallia particles from the silica matrix were observed even in **UCB1-GaSi$_3$** (Fig. 5). This result is consistent with the broadness of the observed pXRD peaks for these materials, and supports previous reports indicating that the presence of pre-formed M[–O–SiO_3]$_n$ linkages in a single-source precursor leads to highly dispersed metal oxides upon thermolysis.[12,25] It is interesting to note that samples with 1 : 3 and 1 : 10 Ga : Si ratios exhibit similar degrees of dispersion despite the differences in pXRD and ^{71}Ga MAS-NMR spectra noted above. This suggests that any phase segregation in the **UCB1-GaSi$_3$** sample occurs on a scale smaller than that observable by elemental mapping without incurring beam damage to the samples. The pixel edge is ~3 nm in length, so it is estimated that oxide particles formed should be no larger than 10 nm in size.

High-angle annular dark-field scanning transmission electron microscopy (HAADF-STEM) images of all samples showed porous structures as expected. However, the high energy of the electron beam and risk of beam-induced damage prevented magnification to an extent that vermicular pore structures previously reported for this type of material would be observable (see ESI, S13†).

While STEM images were unable to provide evidence for structural differences between **UCB1-GaSi** samples, dinitrogen-physisorption measurements clearly indicated changes in porosity. It was observed that as the silicon content increases in the **UCB1-GaSi** materials, surface areas decreases. A shift in the hysteresis loops towards higher P/P_0 values with increasing silica content was also observed, along with changes in the pore radii distributions that showed broader pore size distributions and a shift to higher average radii (Fig. 6). While specific pore structures were unobservable at the magnifications used for STEM, the dinitrogen-physisorption measurements taken of **UCB1-GaSi$_3$** are consistent with earlier reports of UCB1-type materials for which vermicular pores were observable by TEM.[20]

The observation that pore uniformity is reduced with increasing silicon content is noteworthy. The narrow pore distributions of **UCB1** materials were previously attributed to Lewis acid–base interactions between Lewis-acidic metal centers in the molecular precursors and Lewis-basic oxygen atoms of ethylene or propylene glycol monomers in the P-123 Pluronic template.[20] This interaction was proposed to lead to polymer unfolding. This hypothesis was put forth based on a previous report by Soler-Illia and Sanchez, who postulated that under conditions involving limited water the hydrolysis of various transition metal alkoxides to mesoporous materials containing vermicular pores was due to coordination of P-123 Pluronic to the metal precursors.[34] An additional effect presumably results from the role played by the Lewis acid

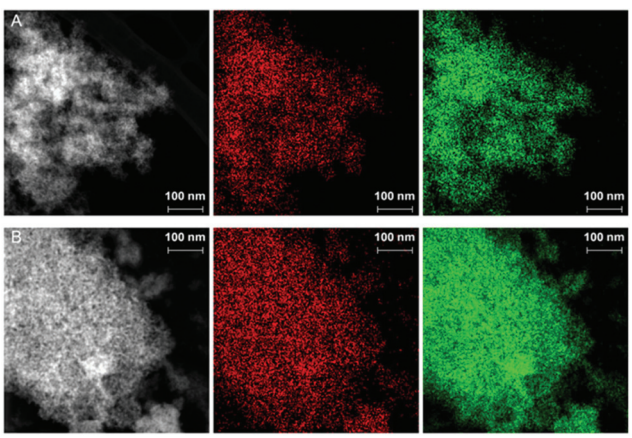

Fig. 5 Elemental maps of (A) **UCB1-GaSi$_3$** and (B) **UCB1-GaSi$_{10}$**. The first column from the left contains HAADF-STEM images of the mapped region. The second (red) and third (green) columns are the Ga and Si channels of the elemental maps, respectively.

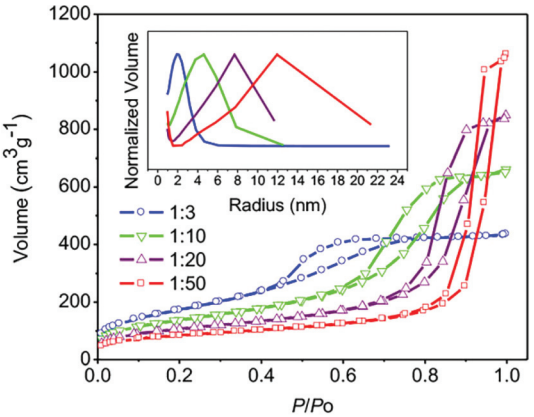

Fig. 6 Nitrogen adsorption–desorption isotherms and pore size distributions (as change in pore volume with respect to pore radius, inset) after calcination at 500 °C in O_2 for **UCB1-GaSi$_3$** (1 : 3), **UCB1-GaSi$_{10}$** (1 : 10), **UCB1-GaSi$_{20}$** (1 : 20), and **UCB1-GaSi$_{50}$** (1 : 50). Pore size distributions are normalized for all samples (for un-normalized figure see ESI, S11†).

concentration, since oxide network formation is catalysed by the acid. Thus, at higher concentrations of Ga the oxide domains condense more rapidly, such that the resulting structure is more strongly influenced by the template. The observation that there is a loss of templating in materials synthesized with lower gallium content is therefore consistent with gallium-based Lewis acid sites playing a significant role in vermicular pore formation.

The observed trend that surface area decreased with increasing silicon content stands in stark contrast to the trends observed in many post-synthetic and sol–gel based methods for generating mesoporous gallium-silica.[27–29] In general, it is found that increasing the loading of a metal by post-synthetic methods leads to lower surface areas due to pore blockage by precursor deposition or, in extreme cases, sintering of metal particles and the formation of metal oxide phases separated from the high-surface area silica support. The materials described here display dramatically different trends in physical characteristics, which suggests that the factors controlling material formation by TMP methods significantly differ from those found in traditional hydrothermal and post-synthetic methodologies (Table 1).

Characterization of surface acidities of UCB1-GaSi materials

Gallium-silica materials are primarily of interest as acid catalysts, therefore, the acidic properties of the materials were probed by ammonia temperature-programmed desorption (NH_3-TPD) and pyridine-FTIR (Table 2). NH_3-TPD measurements provide total acid content including both Lewis and Brønsted acidic sites. Pyridine-FTIR can provide two IR-peaks centered at ~1455 and ~1545, which after correction for integrated molar extinction coefficients (IMEC) give the relative ratios of Brønsted and Lewis acids.[16] The combination of the two methods allows for an estimation of the acidic site densities on the surface when corrected for surface areas.

The Brønsted and Lewis acid site densities measured for **UCB1-GaSi** materials revealed decreased Lewis acid densities and increased Brønsted acid densities as the silicon content increased (Table 2). This can be partially attributed to the gallium oxide observed by ^{71}Ga MAS-NMR that was not apparent in samples with low gallium content. It has been reported that γ-Ga_2O_3 has a high ratio of Lewis acid sites to Brønsted acid sites.[32] In addition, the increasing Brønsted acid concentration with increasing silicon content can be attributed to increased dispersion of the gallium atoms within the silica support. Insertion of Ga^{3+} cations into tetrahedral Si^{4+} positions necessitates protonation of the surface to maintain charge balance. It is possible that gallium hydroxyl species are formed on the surface as well (Fig. 7). On the other extreme, at low silicon content gallium oxide particles formed on the surface may block Brønsted acid sites.

The measured Brønsted acidities are similar to those of mesoporous silica (SBA-15) samples dehydrated under the same conditions (~2 OH^- per nm^2). For reference, the physical limit of hydration for a silica material is estimated at 4.6–4.9 OH per nm^2.[35]

The total acid site densities, as measured by ammonia temperature-programmed desorption, exhibit interesting trends in acid center strengths as indicated by the increased prevalence of moderate strength acid sites and the decreased prevalence of strong acid sites as the gallium content of the material increases. Complex desorption profiles indicate the presence of several types of acid sites in all samples (Fig. 6). At low gallium loadings most of the acidity is associated with both weak (desorption temperature of ~200 °C) and strong (desorption temperature of ~600–700 °C) acid sites, with a small amount of moderate strength sites (desorption temperature of 300–400 °C). Upon inclusion of more gallium, large desorption peaks centered from 300–500 °C suggest that additional gallium generates moderate-strength acid sites (Fig. 8).

While all ammonia desorption traces exhibit similar features below 375 °C, notable differences in desorption peaks are observed at higher temperatures. In **UCB1-GaSi$_3$** a major peak is observed between 450–500 °C that remains only as a trace signal upon dilution of the gallium content in **UCB1-GaSi$_{10}$**. A new major signal is observed at higher temperatures (578 °C) that also appears in even more gallium-poor **UCB1-GaSi$_{20}$** and **UCB1-GaSi$_{50}$** (642 and 622 °C). This suggests the presence of acid sites in **UCB1-GaSi$_3$** that are replaced with stronger sites in more dilute samples.

Several of the ammonia desorption peaks observed for **UCB1-GaSi** materials are similar to previous reports of desorption peaks measured for gallium-containing silicas. Ammonia desorption peaks observed in the range of 100–200 °C have been attributed to weakly acidic Brønsted acid groups and the high temperature peaks from 550–650 °C are tentatively assigned to Brønsted acid sites as well.[36] The broad peaks attributed to moderate strength acid sites with maxima at ~300 °C have been assigned to Lewis acidic structures.[37,38]

Table 2 Acid site densities of **UCB1-GaSi** materials

Material	Total acidity[a] (sites per nm^2)	Bronsted acidity (sites per nm^2)	Lewis acidity (sites per nm^2)
UCB1-GaSi$_3$	4.74	0.9	3.8
UCB1-GaSi$_{10}$	3.89	1.3	2.6
UCB1-GaSi$_{20}$	3.79	1.4	2.4
UCB1-GaSi$_{50}$	4.84	3.0	1.8

[a] Values measured by NH_3-TPD. Bronsted and Lewis acid ratios determined by pyridine-FTIR.

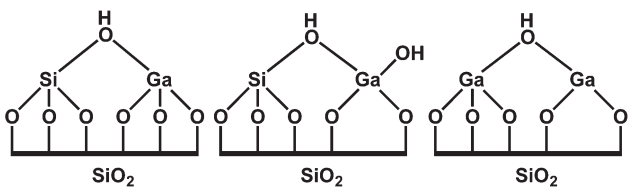

Fig. 7 Possible surface structures of gallium that would contribute to Brønsted acidity.

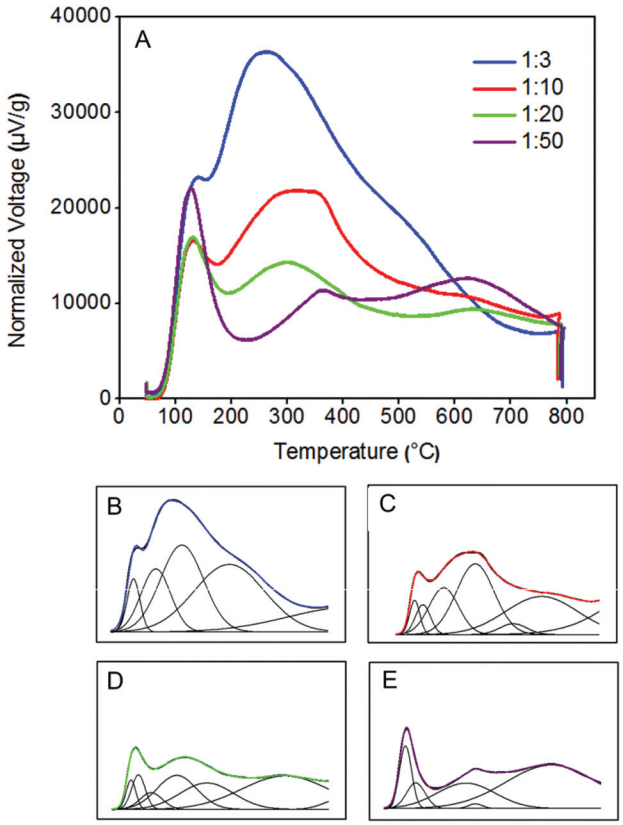

Fig. 8 NH_3-TPD curves and Gaussian curve fits for **UCB1-GaSi$_3$** (1 : 3), **UCB1-GaSi$_{10}$** (1 : 10), **UCB1-GaSi$_{20}$** (1 : 20), and **UCB1-GaSi$_{50}$** (1 : 50). (A) Overlay of all curves showing entire range used for acidity measurements. (B) 1 : 3, 5 peak fit, peak centers (°C): 127, 203, 292, 454, 874. (C) 1 : 10, 7 peak fit, peak centers (°C): 118, 148, 223, 337, 475, 578, 1117. (D) 1 : 20, 7 peak fit, peak centers (°C): 115, 140, 184, 272, 375, 642, 828. (E) 1 : 50, 5 peak fit, peak centers (°C): 123, 158, 330, 362, 622.

Ultimately, the investigation of surface acidities serves to inform the potential application of these materials for catalysis. Initial investigations of **UCB1-GaSi$_3$**, which displays the greatest density of Lewis acid sites, shows promise. Under reaction conditions that have been employed for Friedel–Crafts alkylations (40 °C, N_2, 35 mg catalyst, 3.25 mL benzene, 0.25 mL benzyl chloride), complete conversion of benzyl chloride was achieved within 30 minutes, with 87% selectivity to diphenylmethane. For comparison, Vinu *et al.* reported 100% selectivity and 95% conversion using KIT-6 silica impregnated with 30 wt% Ga_2O_3 nanoparticles; however, even at a higher temperature (50 °C) it took 75 minutes to achieve this conversion.[39] The application of these materials for Lewis acid catalysis is ongoing.

Conclusions

$Ga[OSi(O^tBu)_3]_3$·THF (**1**) is an effective molecular precursor for the synthesis of gallium-silica materials. This is the first example of a molecular gallium silanolate that can be used to generate gallium-silica materials by low temperature thermolysis. Co-thermolysis of **1** with tris(*tert*-butoxy)silanol is possible over a wide range of gallium loadings and the targeted loadings were achievable with a high degree of precision. In addition, the coordination environments of the gallium centers of the final materials may be controlled by varying the relative ratio of **1** and $HOSi(O^tBu)_3$ starting materials. At high gallium content, pXRD and ^{71}Ga MAS-NMR suggest the formation of Ga_2O_3 which is not present when the gallium content is decreased. The precise control of metal loading in these materials could be useful in studying the effects of nuclearity on reactivity. High surface areas were observed in all samples, and, unusually, surface areas increased with increasing gallium content.

Co-thermolysis of **1** with $HOSi(O^tBu)_3$ in the presence of P-123 Pluronic results in the loss of vermicular pore structures as the silicon content increases. Based on literature precedent, it is proposed that the Lewis acid centers coordinate to oxygen centers in the polymer and this interaction, in combination with more rapid thermolysis with more Lewis-acidic gallium centers, is key in templating vermicular pore structures with narrow size distributions.

Acknowledgements

Work at the Molecular Foundry was supported by the Office of Science, Office of Basic Energy Sciences, of the U.S. Department of Energy under Contract No. DE-AC02-05CH11231. We gratefully acknowledge the support of the Director, Office of Energy Research, Office of Basic Energy Sciences, Chemical Sciences Division, of the U.S. Department of Energy (DOE) under Contract DE-AC02-05CH11231. We acknowledge the National Institutes of Health for funding the UC Berkeley CheXray X-ray crystallographic facility under Grant No. S10-RR027172 and the UC Berkeley College of Chemistry NMR facility under Grant No. SRR023679A and 1S10RR016634-01. We acknowledge Neelay Phadke, Dr. Truman C. Wambach and Andy L. Nguyen for helpful discussions. The authors would also like to acknowledge Micah Ziegler for assistance with crystal structure analysis.

Notes and references

1 R. Fricke, H. Kosslick, G. Lischke and M. Richter, *Chem. Rev.*, 2000, **100**, 2303.
2 M. Guisnet and N. S. Gnep, *Catal. Today*, 1996, **31**, 275.
3 E. G. Moschetta, N. A. Brunelli and C. W. Jones, *Appl. Catal., A*, 2015, **504**, 429.
4 S. Mandal, A. SinhaMahapatra, B. Rakesh, R. Kumar, A. Panda and B. Chowdhury, *Catal. Commun.*, 2011, **12**, 734.
5 P. P. Pescarmona and P. A. Jacobs, *Catal. Today*, 2008, **137**, 52.
6 K. Bachari and O. Cherifi, *J. Mol. Catal. A: Chem.*, 2006, **253**, 187.

7 M. J. Gracia, E. Losada, R. Luque, J. M. Campelo, D. Luna, J. M. Marinas and A. A. Romero, *Appl. Catal., A*, 2008, **349**, 148.
8 A. E. Ahmed and F. Adam, *Microporous Mesoporous Mater.*, 2009, **118**, 35.
9 K. Samedov, Y. Aksu and M. Driess, *ChemPlusChem*, 2012, **77**, 663.
10 D. Solis-Ibarra, M. de J. Velásquez-Hernández, R. Huerta-Lavorie and V. Jancik, *Inorg. Chem.*, 2011, **50**, 8907.
11 (*a*) K. W. Terry, C. G. Lugmair and T. D. Tilley, *J. Am. Chem. Soc.*, 1997, **119**, 9745; (*b*) K. L. Fujdala and T. D. Tilley, *J. Catal.*, 2003, **216**, 265.
12 (*a*) J. W. Kriesel and T. D. Tilley, *J. Mater. Chem.*, 2001, **11**, 1081; (*b*) K. L. Fujdala, R. L. Brutchey and T. D. Tilley, *Top. Organomet. Chem.*, 2005, **16**, 69; (*c*) T. D. Tilley, *J. Mol. Catal. A: Chem.*, 2002, **182–183**, 17; (*d*) D. A. Ruddy and T. D. Tilley, *J. Am. Chem. Soc.*, 2008, **130**, 11088; (*e*) C. Copéret, A. Comas-Vives, M. P. Conley, D. P. Estes, A. Fedorov, V. Mougel, H. Nagae, F. Núñez-Zarur and P. A. Zhizhko, *Chem. Rev.*, 2016, **116**, 323; (*f*) K. L. Fujdala and T. D. Tilley, *J. Am. Chem. Soc.*, 2001, **123**, 10133.
13 Y. Abe and I. Kijima, *Bull. Chem. Soc. Jpn.*, 1969, **42**, 1118.
14 M. Kruk, M. Jaroniec, C. H. Ko and R. Ryoo, *Chem. Mater.*, 2000, **12**, 1961.
15 B. Chakraborty and B. Viswanathan, *Catal. Today*, 1999, **49**, 253.
16 C. A. Emeis, *J. Catal.*, 1993, **141**, 347.
17 K. L. Fujdala, A. G. Oliver, F. J. Hollander and T. D. Tilley, *Inorg. Chem.*, 2003, **42**, 1140.
18 C. G. Lugmair, K. L. Fujdala and T. D. Tilley, *Chem. Mater.*, 2002, **14**, 888.
19 K. W. Terry, P. K. Ganzel and T. D. Tilley, *Chem. Mater.*, 1992, **4**, 1290.
20 J. W. Kriesel, M. S. Sander and T. D. Tilley, *Chem. Mater.*, 2001, **13**, 3554.
21 K. S. W. Sing, D. H. Everett, R. A. W. Haul, L. Moscou, R. A. Pierotti, J. Rouquérol and T. Siemieniewska, *Pure Appl. Chem.*, 1985, **57**, 603.
22 (*a*) M. Hirano, K. Sakoda and Y. Hirose, *J. Sol-Gel Sci. Technol.*, 2016, **77**, 348; (*b*) B. Zheng, W. Hua, Y. Yue and Z. Gao, *J. Catal.*, 2005, **232**, 143; (*c*) H. Y. Playford, A. C. Hannon, E. R. Barney and R. I. Walton, *Chem. – Eur. J.*, 2013, **19**, 2803.
23 D. Zhao, J. Feng, Q. Huo, N. Melosh, G. H. Fredrickson, B. F. Chmelka and G. D. Stucky, *Science*, 1998, **279**, 548.
24 V. N. Sigaev, N. V. Golubev, E. S. Ignat'eva, B. Champagnon, D. Vouagner, E. Nardou, R. Lorenzi and A. Paleari, *Nanoscale*, 2013, **5**, 299.
25 R. L. Brutchey, C. G. Lugmair, L. O. Schebaum and T. D. Tilley, *J. Catal.*, 2005, **229**, 72.
26 C.-F. Cheng, H. He, W. Zhou, J. Klinowski, J. A. S. Gonçalves and L. F. Gladden, *J. Phys. Chem.*, 1996, **100**, 390.
27 Z. El Berrichi, B. Louis, J. P. Tessonnier, O. Ersen, L. Cherif, M. J. Ledoux and C. Pham-Huu, *Appl. Catal., A*, 2007, **316**, 219.
28 M. Selvaraj and S. Kawi, *Catal. Today*, 2008, **131**, 82.
29 M. Chatterjee, T. Iwasaki, Y. Onodera, T. Nagase, H. Hayashi and T. Ebina, *Chem. Mater.*, 2000, **12**, 1654.
30 H. J. Backer and H. A. Klasens, *Recl. Trav. Chim. Pays-Bas.*, 1942, **61**, 500.
31 R. L. Brutchey, J. E. Goldberger, T. S. Koffas and T. D. Tilley, *Chem. Mater.*, 2003, **15**, 1040.
32 W. Lueangchaichaweng, N. R. Brooks, S. Fiorilli, E. Gobechiya, K. Lin, L. Li, S. Parres-Esclapez, E. Javon, S. Bals, G. Van Tendeloo, J. A. Martens, C. E. A. Kirschhock, P. A. Jacobs and P. P. Pescarmona, *Angew. Chem., Int. Ed.*, 2014, **53**, 1585.
33 L. A. O'Dell, S. L. P. Savin, A. V. Chadwick and M. E. Smith, *Appl. Magn. Reson.*, 2007, **32**, 527.
34 G. J. de A. A. Soler-Illia and C. Sanchez, *New J. Chem.*, 2000, **24**, 493.
35 L. T. Zhuravlev, *Colloids Surf., A*, 2000, **173**, 1.
36 T. Takeguchi, J. Kim, M. Kang, T. Inui, W. Cheuh and G. L. Haller, *J. Catal.*, 1998, **175**, 1.
37 B. Karmakar, A. Sinhamahapatra, A. B. Panda, J. Banerji and B. Chowdhury, *Appl. Catal., A*, 2011, **392**, 111.
38 S. J. Kim, K.-D. Jung and O.-S. Joo, *J. Porous Mater.*, 2004, **11**, 211.
39 H. Oveisi, C. Anand, A. Mano, S. S. Al-Deyab, P. Kalita, A. Beitollahi and A. Vinu, *J. Mater. Chem.*, 2010, **20**, 10120.